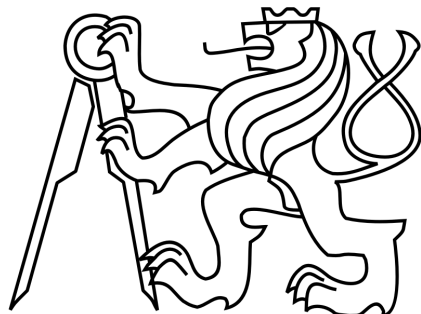


CZECH TECHNICAL UNIVERSITY IN PRAGUE
Faculty of Civil Engineering
Department of Mechanics



Application of Boundary Inverse Methods in
Civil Engineering

DOCTORAL THESIS STATEMENT

Ing. Jan Havelka

Prague 2017

Název práce:	Aplikace hraničních inverzních metod ve stavebním inženýrství
Autor:	Ing. Jan Havelka
Vedoucí práce:	Ing. Jan Sýkora, Ph.D.
Studijní program:	Stavební inženýrství
Obor studia:	Fyzikální a materiálové inženýrství

Abstrakt

V určitých oblastech výzkumu, jako například analýza historických budov, zobrazovací techniky v medicíně, materiálové inženýrství, geofyzika a ostatní, je výhodné provádět pouze neintruzivní měření na hranici. Záměrem je získat detailní informace o materiálových vlastnostech uvnitř zkoumaného vzorku při jeho současném neporušení. Tato práce se věnuje právě takovým metodám, které spojují matematický model a inverzní procedury využívající pouze hraniční měření. Celkem se v této tezi uvažují tři výpočetní modely řešící ustálené vedení tepla, elektrostatiku a časově závislé vedení tepla. Jednotlivé modely jsou řešeny pomocí Metody Konečných Prvků (MKP) a pro inverzní analýzu získávání neznámých parametrů je využito modifikovaných Calderónových principů s numerickým řešením pomocí Gauss-Newtonovy metody. Jsou popsány základní principy, detailly o implementaci a modifikace obecných omezení původně odvozených pro standardní Celdérónův problém. Navrhované modely jsou následně numericky ověřeny pro širokou škálu materiálových vlastností, tvarů zkoumaných oblastí a zatěžovacích podmínek.

Klíčová slova

Calderónův problém, Künzelův model, metoda konečných prvků, sdružené vedení tepla a vlhkosti, difúzní rovnice, hraniční inverzní metody, Neumann-to-Dirichlet mapa.

Title:	Application of boundary inverse methods in Civil Engineering
Author:	Ing. Jan Havelka
Supervisor:	Ing. Jan Sýkora, Ph.D.
Doctoral programme:	Civil Engineering
Branch of study:	Physical and Material Engineering

Abstract

In specific fields of research such as treatment of historical structures, medical imaging, material science, geophysics and others, it is of particular interest to perform only a non-intrusive boundary measurement. The idea is to obtain a comprehensive information about the material properties inside the domain under consideration while maintaining the test sample intact. This statement is focused on such problems i.e. synthesizing a physical model of interest with a boundary inverse techniques. The forward model is represented by three diffusion based models with Finite Element (FE) discretisation and the parameters are subsequently recovered using a modified Calderón problem principles which is numerically solved by a regularised Gauss-Newton method. We provide a basic framework, implementation details and modification of general constraints originally derived for a standard setup of Calderón problem. The proposed model setup was numerically verified for various domains, load conditions and material field distributions. Both steady-state and time dependent cases are studied.

Keywords

Calderón problem, Künzel model, Finite Element Method, coupled heat and moisture transport, diffusion equation, boundary inverse method, Neumann-to-Dirichlet map.

Contents

1	Introduction	1
2	Inverse problem	3
2.1	General procedures	4
2.1.1	Deterministic methods	4
2.1.2	Probabilistic methods	6
3	Calderón problem	8
3.1	Problem definition	9
4	Forward models	11
4.1	Electrical Impedance Tomography	11
4.2	General Transport Model (GTM) application	14
4.3	Time dependent heat equation	16
4.4	Numerical solution to the inverse problem	19
5	Results	21
5.1	Electrical Impedance Tomography	22
5.2	General Transport Model	24
5.3	Time dependent heat equation	27
6	Summary and future work	29
References		i

1 Introduction

Numerical methods have become an inherent part of engineering designs. Not only they serve as a prediction of the system behaviour but are also able to provide a complex information about the genuine interaction of individual components. Together with the ever increasing computer performance it opens up the possibilities for an extensive optimisation based designs resulting into energy, material, human resources and time savings. However, the precision of a model response compared to the real observations often varies to some extent. Since every mathematical model is a collection of theoretical knowledge and principles, errors due to an approximation on the physical phenomena level, material description, loading conditions etc. contribute to the gap between the actual observation and model prediction. In a pursuit of matching the relation between reality and model response, one can find several ways for eliminating the observable discrepancy. Each direction inevitably induces another trade off to harness embodied in a balance between computational complexity, model simplicity, number of parameters and additional decision making whether the increased complexity is worth the effort. Despite the difficulties, however, the trend is today in favour of more complex models due to the progress in manufacturing precision, profound development in numerical procedures, accurate measurement techniques and increasing computational power. In following paragraphs we shall briefly outline the main options for improving the model precision in order to better reflect the real physical processes while we will mainly focus on models applicable in civil engineering, e.g. problems mainly governed by elliptic or parabolic partial differential equations (PDEs) with defined geometric, load and material properties.

The first strategy treats the fundamental model description by examining various environmental factors and their interactions. The result of including new relations can be represented by a coupled models, e.g. fire-structure analysis [61], moisture-heat transport [45], climate models [28] and other multi-physics problems. Another example of modification at the level of governing equations can be introduction of geometric non-linearity, which can occur due to large displacements, strains, rotations, etc.

The second option is to modify the constitutive law, i.e. to treat the relations on material description level. This includes a wide area of application ranging from modelling unsaturated environment in a ground water flow [80] through damage [7] and plasticity [85, 39] to various forms of ageing like creep or relaxation [8] in structures. Since the material property often depends on state variables, the model itself becomes non-linear.

The third strategy combines the outer effects, i.e. the boundary or load

conditions, together with the problem of handling errors due to the physical domain deviations, discrepancy between the real and simulated load conditions, material properties, etc. This most frequently involves the probabilistic approach [29, 51], admitting the randomness to occur on all aforementioned levels allowing to study the impact of many sources of uncertainties on the model response.

Essentially, the majority of foregoing strategies enriches the model with additional information by increasing the number of parameters and computational complexity. Such models require a broad knowledge and understanding of the input parameters which is often accomplished by an in many cases expensive experiment of dubious precision. This statement provides an insight into a boundary inverse technique which is allowing to perform a non-invasive measurements that admits to maintain the sample object under consideration intact meanwhile providing comprehensive information about the parameters distribution inside the observed object.

2 Inverse problem

In a classical concept of numerical analysis, one is often provided with an appropriate physical model and a certain environment which it is subjected to, i.e. a set of possible causes with a knowledge of the system behaviour, and subsequently try to calculate the model response. Such a procedure is called a forward model and is opposite to the inverse problem, for which the main objective is to determine the cause from a given observations. Generally, in the sense of Hadamard the most forward models for physical situations lead to a well-posed problems [32] for which the conditions can be stated as

- for all admissible data the solution exists (existence),
- for all admissible data there is at most one solution of the problem (uniqueness),
- the solution depends continuously on the data (stability).

However, inverse problems do not necessarily have the aforementioned properties. Solution of such problems might therefore not be unique or stable and even a small changes in the input data can result into a large changes in the solution violating the third condition and the problem can be therefore recognised to be ill-posed [81, 42]. Another criterion that comes into consideration is uniqueness of the solution which can be better understood as a possible information shortage or data insufficiency and will be discussed further in section 3.

Although lack of the information cannot be remedied by any mathematical treatment [47], stability of the solution can be treated by various mathematical procedures. In case the instability is intrinsic property of the system itself and the problem can not be reformulated, one needs to provide the system with additional assumptions, e.g. some prior information, enforce smoothness, prefer solution with the smallest norm, provide bounds to the unknown entity, etc. Procedures for determining the constraints and solving such problems are generally called regularisation methods and within this statement are categorised as deterministic and statistical with a brief overview of frequently used methods in following subsections.

Despite the aforementioned difficulties, inverse problems represent one of the most important topics in mathematics and have a wide range of applications in medical imaging [79, 3, 23, 22, 5, 34], geophysics [59, 27, 83, 48, 68, 69], machine learning [70, 78], acoustics[64, 24, 78], signal processing [60] and many other fields.

2.1 General procedures

Since the numerical procedures for solving ill-posed and non-linear problems are mathematically identical for various problems, boundary inverse methods can be therefore solved in number of ways. The traditional approach is to linearise the problem and subsequently use a regularisation method to stabilize the solver. The resulting system can be then evaluated iteratively by one from family of Newton-type methods. The opportunity to perform regularisation of the problem prior to linearisation or vice versa opens up a wide range of possible ways to solve such problems.

The minimisation problem is often stated as follows, with the first term representing the cost function and the second term being the regularisation penalty

$$\sigma_r = \arg \min_{\sigma} \|F(\sigma) - \mathbf{u}_m\|_p + G(\sigma), \quad (2.1)$$

where $F(\sigma)$ is the output of the forward operator, \mathbf{u}_m is the vector of measured quantity, $G(\sigma)$ is the regularisation functional, introducing the additional constraints to the solution, σ_r is the parameter field being reconstructed and p indicates ℓ_p -norm.

2.1.1 Deterministic methods

Since the reconstruction methods in various fields are pursuing different interests, e.g. the interest in non-iterative methods is mostly driven by the necessity of fast and reliable reconstruction algorithms generating real time visualisations in medical imaging [33, 72], whereas in geophysics [19, 48, 35], one can make use of iterative algorithms with the ability to provide generally more refined solutions.

Deterministic regularisation procedures can be therefore further divided into non-iterative linearisation based methods, e.g. back-projection methods [65, 9], Calderón's approach [12], moment methods [2] and one-step Newton family methods [11, 55, 20], which all are based on the assumption of small perturbations of the parameter field. The linearisation of a forward operator in such methods is usually expressed in a following way

$$F(\sigma) \approx F(\sigma_0) + J(\sigma - \sigma_0), \quad (2.2)$$

where J is the Jacobian matrix of F , evaluated at σ_0 .

A typical choice of the regularisation penalty term in Eq. (2.1) is of following form [81]

$$G(\sigma) = \alpha^2 \|\mathbf{L}(\sigma - \sigma_0)\|_{\ell_2}^2, \quad (2.3)$$

where the hyper-parameter, i.e. regularisation parameter, α is controlling the trade-off between solution stability, given constraints and a distance from the true solution. An additional constrain σ_r represents some known and possibly non-smooth behaviour of the unknown parameter [35]. A straightforward way of explaining the regularisation operator \mathbf{L} is such that it draws the solution towards its null space, i.e. $\ker(\mathbf{L})$. It might take form of a discrete approximation to the Laplacian¹ of a piecewise constant functions on the finite element mesh [82], a weighted diagonal matrix to promote a sparse solution [25], Gaussian smoothing filter [13] or without any knowledge of the system, the operator is often left to be an identity.

A different approach is represented by the non-iterative fully non-linear methods, from which the layer stripping method [72] was introduced as the first one. A more recent development is then devoted to scattering transform, i.e. D-Bar or $\bar{\partial}$ methods [67, 44], due to its ability to accurately recover the absolute conductivity field and handle various noise levels. Furthermore the method was extended to the third dimension [10].

The probably best known and understood methods are iterative algorithms which often make use of Tikhonov regularisation. In a classical settings, the penalty term takes a following form

$$G(\sigma) = \alpha^2 \|\mathbf{L}(\sigma)\|_{\ell_2}^2. \quad (2.4)$$

In general, both terms in Eq. (2.1) are preferred to be ℓ_2 -norm due to the convenience for computational purposes and preference of smooth solutions [52]. In such case, by combining the minimisation scheme Eq. (2.1) for $p = 2$, linearised forward operator Eq. (2.2), penalty term Eq. (2.3) and a Gauss-Newton approximation of Newton-Raphson multi-variable method, one can obtain a following iterative formula [35]

$$\sigma_{k+1} = \sigma_k + \left(\mathbf{J}_k^T \mathbf{J}_k + \alpha^2 \mathbf{L}^T \mathbf{L} \right)^{-1} \left(\mathbf{J}_k^T (\mathbf{u}_m - F(\sigma_k)) - \alpha^2 \mathbf{L}^T \mathbf{L} (\sigma_k - \sigma_0) \right), \quad (2.5)$$

where \mathbf{J}_k is the Jacobian evaluated at σ_k .

A different approach is to use so called Total Variation (TV) functional in the penalty term, i.e. to replace ℓ_2 -norm with ℓ_1 -norm:

$$G(\sigma) = \alpha \|\mathbf{L}(\sigma - \sigma_r)\|_{\ell_1} \quad (2.6)$$

¹The null space of such operator is any constant field or more precisely the solution is pushed towards solution $\sigma_s = \sigma_r + c$, where $c \in \mathbb{R}$ is constant shift of the whole field in any direction.

With following consequences regarding the solution: the resulting parameter σ is more strictly tightened to the exact solution, allowing to preserve sharp edges, represent piece-wise constant solutions and other desirable properties, e.g. handling a moderate levels of noise [62, 14]. However implementation of TV functional is not straightforward due to its non-differentiability [52], requiring to use a non-standard solvers, e.g. deterministic Lagged Diffusivity Method (LDM) using a hybrid ℓ_1/ℓ_2 , the Primal Dual-Interior Point Method (PDIPM) [52] using a true ℓ_1 or probabilistic methods such as Markov Chain Monte Carlo (MCMC) [46, 73] algorithm.

Despite nearly every regularisation technique requires a choice of a hyper-parameter, there is not yet a rigorous formulation with guaranteed convergence and stability. However there are various ad-hoc methods, e.g. heuristic selection, L-Curve method, Generalised Cross-Validation (GCV), Fixed Noise Figure (NF), discrepancy principle or Greferer/Raus method [81, 30].

2.1.2 Probabilistic methods

Although the models we intend to use are not considered to be strictly random in nature, one can still benefit from recasting the problem by treating the individual unknown parameters as random variables, i.e. reformulating the problem to a form of statistical inference. The parameter randomness represents an extension to the traditional deterministic approach and can be viewed as the uncertainty to its true value expressed by the means of a probability distribution. Most often the statistical inference is based on the notion of conditional probabilities which gives rise to Bayesian approach in a following form

$$p(\mathbf{m}|\mathbf{z}) = \frac{p(\mathbf{z}|\mathbf{m})}{p(\mathbf{z})} \cdot p(\mathbf{m}), \quad (2.7)$$

where solution is the *posterior* probability distribution $p(\mathbf{m}|\mathbf{z})$ of the unknown parameter \mathbf{m} conditioned on the provided measurements \mathbf{z} , $p(\mathbf{z}|\mathbf{m})$ is the *likelihood*, i.e. the conditional probability of \mathbf{z} assuming that \mathbf{m} is given. The *evidence* $p(\mathbf{z})$ represents the probability of observing \mathbf{z} and the *prior* $p(\mathbf{m})$ relates to what is known prior to observing the data \mathbf{z} [53].

Once knowing the posterior density, one can obtain several forecasts of the unknown parameters by evaluating the point estimates, i.e. mean, median, maximum, etc.

Taking the mean estimate, one obtain a Minimum Mean Square Estimation (MMSE) enforcing the minimisation of the square norm of estimate error, i.e.

$$\tilde{\mathbf{m}}_{MS}(\mathbf{z}) = \arg \min_{\tilde{\mathbf{m}}} \mathbb{E} \{ \|\mathbf{m} - \tilde{\mathbf{m}}(\mathbf{z})\|_2 \}, \quad (2.8)$$

where an estimator $\tilde{\mathbf{m}}(\mathbf{z})$ of \mathbf{m} is any function of the measurement \mathbf{z} . With the help of Bayesian cost method [54] the MMSE can be obtained as a conditional expectation of \mathbf{m} given the measurements \mathbf{z} , i.e. the estimator is given by the posterior mean of the parameter to be estimated.

$$\tilde{\mathbf{m}}_{MS} = \int_{-\infty}^{\infty} \mathbf{m} p(\mathbf{m}|\mathbf{z}) d\mathbf{m} = \mathbb{E} \{ \mathbf{m} | \mathbf{z} \} \quad (2.9)$$

In Maximum Likelihood Estimation (MLE) one is trying to find a set of parameters $\mathbf{m}_{MLE}(\mathbf{z})$ for given data \mathbf{z} such that the maximum likelihood satisfy

$$p(\mathbf{z} | \mathbf{m}_{MLE}) \geq p(\mathbf{z} | \mathbf{m}), \quad (2.10)$$

i.e. \mathbf{m}_{MLE} makes the observation \mathbf{z} most probable and maximizes the likelihood function $p(\mathbf{z} | \mathbf{m})$ [81, 54].

In Maximum a Posteriori (MAP) an estimation is based on maximum of the posterior conditional density $p(\mathbf{m} | \mathbf{z})$ which is obtained by integrating conditional expectation which, especially for large parameter spaces, often make use of Monte Carlo (MC) methods, such as Markov chain Monte Carlo (MCMC). With Gaussian assumptions of prior and likelihood, the MAP estimator is identical to MMSE and ML.

3 Calderón problem

Many disciplines ranging from geophysics to medicine has a common denominator, which is the principle that is being named after Argentinian mathematician Alberto Calderón, who first formed his thoughts in a foundational paper [17, 18] published in 1980. Although the first signs of similar works dates back to the 1930s in geophysics [48, 69], Calderón was the first who defined a more profound mathematical formulation.

Nowadays one of the most common application utilizing Calderón problem principles is Electrical Impedance Tomography (EIT). As a medical imaging technique it was proposed earlier in 1978 by John G. Webster [34]. The first tomogram was constructed later in 1983 by David C. Barber and Brian H. Brown and further details were described in their joint work in 1984 [5]. The basic idea of this method lies in the difference of surface measurements due to the variations in the subsurface conductivity distribution. Meanwhile a single set of surface measurements for a given loading conditions might result in a number of possible conductivity fields, Calderón surpassed this problem by sequentially implying multiple current patterns², i.e. loading conditions, which yields into a unique conductivity distribution. The crucial part of successful material field recovery is a precision placement of measurement electrodes together with boundary shape and knowledge of loading conditions, i.e. knowing an impedance³ and the current flow.

This non-invasive and painless method has gained its popularity mainly due to its inexpensiveness, portability and the rate in which it is able to evaluate results, which can be up to 1000 frames per second [83]. As a medical imaging technique it is used e.g. for lung examination and respiratory problems [15, 49], as an alternative technique to mammography [23, 22], monitoring brain activity [79, 3] etc.

A similar technique used in geophysics is Electrical Resistivity Tomography (ERT) or Electrical Resistivity Imaging (ERI). In contrast to EIT the electrodes are not usually placed on the ground surface, but are often inserted into vertical boreholes filled with water. Otherwise the mathematical formulation and inverse procedure is identical to the one used in EIT. A more modern concept of ERT is used to capture fluid movement in porous [27, 26] and fractured [68] media. Another interesting application of this method is in archaeology [59], where it is used to roughly locate possible findings.

Least used application similar to EIT awaiting for a more widespread use is Electrical Capacitance Tomography (ECT) [84, 36]. The industrial

²Each current pattern (CP) yields in another set of measurements

³An impedance can be in direct current (DC) understood as a resistivity to a current flow.

potential use is in monitoring and analysing pneumatic conveying systems, i.e. gas-solid flow [38], measurement of flow of fluids in pipes [36] and measurement of the concentration of one fluid in another, or the distribution of a solid in a fluid.

However the major downside of this method lies in its spatial resolution which is several orders of magnitude lower in comparison to other imaging techniques such as Computed Tomography (CT) or Magnetic Resonance Imaging (MRI). Another problem to harness is the need of additional data processing in order to recover the final image and handling the deviations in real and simulated boundary shape etc.

The ongoing research focusses essentially on two main problems. The first is being the possibility of recovering an anisotropic conductivity tensor field for which it is known to suffer from insufficiency of data and can not be in general uniquely determined by boundary data [31]. This can be however remedied by a sufficient a priori knowledge [50]. A different approach to solve this problem can be found in following papers [4, 33]. Another important direction of development is the work on reconstruction algorithms and advanced numerical methods.

3.1 Problem definition

Mathematically the Calderón's inverse problem represents a non-linear and severely ill-posed problem [56, 77] of recovering a coefficient of divergence in a system of elliptic partial differential equations. For electrostatic EIT the problem is modelled by the generalised Laplace equation with following boundary conditions

$$\begin{cases} \nabla \cdot (\sigma \nabla u) = 0, & \text{in } \Omega \\ \sigma \nabla_x u \cdot n = f, & \text{on } \partial\Omega \\ \int_{\partial\Omega} u dS = 0, \end{cases} \quad (3.1)$$

where $f \in H^{-1/2}(\partial\Omega)$ is a given current flux on the boundary $\partial\Omega$ and the induced potential $u \in H^1(\Omega)$ uniquely solves the Neumann boundary value problem in a bounded domain $\Omega \subseteq \mathbb{R}^2$. The electrical conductivity σ is assumed to be scalar valued, strictly positive and bounded in Ω .

The knowledge of resulting potential distribution $u \in H^{1/2}(\partial\Omega)$ then gives rise to the Neumann-to-Dirichlet (NTD) $\Lambda_\sigma : H^{-1/2}(\partial\Omega) \rightarrow H^{1/2}(\partial\Omega)$ map, which can be formally defined as

$$\Lambda_\sigma : (\sigma \nabla u) \cdot n|_{\partial\Omega} \rightarrow u|_{\partial\Omega}. \quad (3.2)$$

Conversely, given $g \in H^{1/2}(\partial\Omega)$ Dirichlet boundary data and observing the resulting current density distribution on the boundary $\partial\Omega$, one can define Dirichlet-to-Neumann (NTD) $\Lambda_\sigma^{-1} : H^{1/2}(\partial\Omega) \rightarrow H^{-1/2}(\partial\Omega)$ map as

$$\Lambda_\sigma^{-1} : u|_{\partial\Omega} \rightarrow (\sigma \nabla u) \cdot n|_{\partial\Omega}. \quad (3.3)$$

With this definition Λ_σ and Λ_σ^{-1} are bounded linear maps though non-linearly depending on the conductivity σ . The physical representation of NTD map can be interpreted as knowledge of the resulting potential distribution on $\partial\Omega$ corresponding to given flux distribution on $\partial\Omega$.

The problem of interest is then to ask whether the Cauchy data Λ_σ or Λ_σ^{-1} determines the conductivity σ in Ω uniquely. The injectivity of forward map Eq. (3.4) and uniqueness were proven under variety of assumptions in [76, 57, 71, 16].

$$\lambda_{\sigma_1} = \lambda_{\sigma_2} \Rightarrow \sigma_1 = \sigma_2 \quad (3.4)$$

From practical point of view the recovery process suffers from limited number of independent measurements, its accuracy and large number of degrees of freedom of a parametrised conductivity to be identified. Although the solution stability has been studied [1, 63], partial data recovery still remains to be an opened question [40, 43, 41] and is numerically studied in section 5.

4 Forward models

Throughout this thesis, we will consider three pervading numerical models which, although with different physical interpretations are based on a diffusion equation. Numerical models will play a fundamental role since each will be repeatedly used in the inverse process and will also substitute an experiment. Numerical solutions of each model are always obtained using Finite Element Method (FEM) [6, 37, 74, 85]. The space-time discretisation and other specifications are briefly outlined for each model within its section.

4.1 Electrical Impedance Tomography

There exist a number of established forward models whether for direct or alternating current, assuming various simplifications with a different computational complexity. In this thesis we will mainly concentrate on direct current models as they are closely related to the processes in civil engineering environment. The simplest models can be represented by a *continuum*, *shunt* or *gap model*, which are sometimes referred to as a non-physical, due to the simplification in modelling the electrode as a perfectly conducting single point, e.g. there is no transition impedance between the skin and the actual electrode [66].

A more commonly used *Complete Electrode Model* (CEM) allows to consider electrodes actual physical size and introduces a contact impedance layer between the skin and the electrode. The model was introduced and experimentally validated in 1989 by K. S. Chen [21]. Further proof for CEM solution uniqueness under assumptions 1 was given by E. Somersalo, et al. in 1992 [71]. Significant contributions to the theory were papers [16, 76] proving the solution is uniquely determined in dimension $n \geq 3$ for complete DTN Eq. (3.3) or NTD Eq. (3.2) data. Unlike in $n \geq 3$, in dimension $n = 2$ the problem is undetermined and the solution was proved to be unique up to a change of coordinates [75, 57].

Further in this thesis we will consider only a CEM model, which is defined in a following way

$$\left\{ \begin{array}{l} \nabla \cdot (\sigma(x) \nabla u(x)) = 0, \quad x \in \Omega \\ \int_{e_l} \sigma \frac{\partial u}{\partial n} dS = I_l, \quad l = 1, \dots, L \\ \sigma(x) \frac{\partial u}{\partial n}(x) = 0, \quad x \in \partial\Omega \setminus \bigcup_{l=1}^L e_l \\ u(x) + z_l \sigma(x) \frac{\partial u}{\partial n}(x) = V_l, \quad x \in e_l, l = 1, \dots, L, \end{array} \right. \quad (4.1)$$

where $\Omega \subseteq \mathbb{R}^d$, $d = 2$ is an open bounded set representing the domain with electrical conductivity field $\sigma(x)$ [$\text{A} \cdot \text{V}^{-1}$]. The model consists of L $[-]$ electrodes $(e_l)_{l=1}^L$ $[-]$ attached to the surface $\partial\Omega$, each with contact impedance $(z_l)_{l=1}^L$ $[\Omega]$. Current pattern applied to the electrodes is denoted by $(I_l)_{l=1}^L \in \mathbb{R}^L$ [A]. The electrostatic potential field within the domain is denoted by $u(x)$ [V] and each electrode potential by $(V_l)_{l=1}^L \in \mathbb{R}^L$ [V].

The inputs for this model are the conductivity field $\sigma(x)$, current patterns $(I_l)_{l=1}^L \in \mathbb{R}^L$ and contact impedances $(z_l)_{l=1}^L$. The model output consists of a measurement set $(V_l)_{l=1}^L \in \mathbb{R}^L$ and a potential field $u(x)$.

The model conditions in Eq. (4.1) can be translated as follows: omitting the first term which is the governing equation, the second condition states that the current flux I_j^j is averaged across the active electrode e_j . Third condition states that there is no current leakage through bare skin, assuming the air is an insulator and the last term is a Robin condition, which is representing the existence of an impedance layer and is simulating a constant potential on the electrode while admitting a potential change on the skin underneath the electrode.

The unique solution is proved under following assumptions [71]

Assumption 1. *The conductivity σ , current pattern I_l and the contact impedances z_l satisfy following*

$$(i) \quad \sigma \in L^\infty(\Omega; \mathbb{R}), \quad \inf_{x \in \Omega} \sigma(x) = \sigma_- > 0,$$

$$(ii) \quad 0 < z_- \leq z_l \leq z_+ < \infty, \quad l = 1, \dots, L,$$

$$(iii) \quad \sum_{l=1}^L I_l = 0,$$

$$(iv) \quad \sum_{l=1}^L V_l = 0.$$

Although there are various current pattern strategies [81], it is satisfactory to choose only $L - 1$ linearly independent loading conditions to generate measurements comprising all possible information⁴ due to the linear relationship between current and potential. In our case, the current patterns $I = (I_j)_{j=1}^{L-1} \in \mathbb{R}^{L \times (L-1)}$ takes following form

⁴In case of admitting errors in measurements, redundant current patterns can actually provide additional information.

$$I = C \times \begin{bmatrix} +1 & 0 & \cdots & 0 \\ -1 & +1 & \cdots & 0 \\ 0 & -1 & \ddots & 0 \\ \vdots & \vdots & \ddots & +1 \\ 0 & 0 & 0 & -1 \end{bmatrix}, \quad (4.2)$$

where C [A] is a constant regarding to applied current and each column represents a single load condition. Note also that each loading condition have to sum up to zero, satisfying conditions (iii) and (iv) in assumption 1, with a physical meaning of conservation of charge and choice of ground voltage respectively.

Numerical solution of the forward model

The additional complexity in solving the CEM forward model lies in the property of each electrode, i.e. the impedance and dimensionality. Since the currents and potentials are subsequently transmitted or read through each electrode which is departed from the model via impedance layer, one have to adopt some post-processing or incorporate a virtual electrode nodes to the FE problem in order to obtain full solution. In this statement we followed the usual way of solving this problem which is the latter. The forward operator is then constructed in a following way

$$F(\sigma) = \mathbf{V}, \quad \mathbf{V} \in \mathbb{R}^{L \times (L-1)}, \quad (4.3)$$

where \mathbf{V} is a matrix containing L measurements, i.e. voltages, for $(L - 1)$ individual current stimulation patterns. The set of measurements \mathbf{V} is obtained by solving following set of equations

$$\begin{bmatrix} \mathbf{K} + \mathbf{K}_{uu} & \mathbf{K}_{uv} \\ \mathbf{K}_{uv}^T & \mathbf{K}_{vv} \end{bmatrix} \begin{bmatrix} \mathbf{u} \\ \mathbf{V} \end{bmatrix} = \begin{bmatrix} \mathbf{0} \\ \mathbf{I} \end{bmatrix}, \quad (4.4)$$

where $\mathbf{u} \in \mathbb{R}^{N \times (L-1)}$ is a solution matrix of potentials in Ω , $\mathbf{I} \in \mathbb{R}^{L \times (L-1)}$ is a matrix of current stimulation patterns and the individual system matrices are calculated in a following way

$$K_{ij} = \int_{\Omega} \sigma \nabla \phi_i \cdot \nabla \phi_j \, dA \quad i, j = 1 : N \quad (4.5)$$

$$K_{uu,ij} = \sum_{l=1}^L \int_{e_l} \frac{1}{z_l} \phi_i \phi_j \, dS \quad i, j = 1 : N \quad (4.6)$$

$$K_{uv,il} = - \sum_{l=1}^L \int_{e_l} \frac{1}{z_l} \phi_i \, dS \quad i = 1 : N, l = 1 : L \quad (4.7)$$

$$K_{vv,kl} = \int_{e_l} \frac{1}{z_l} \, dS = \frac{|e_l|}{z_l} \delta_{kl} \quad k, l = 1 : L, \quad (4.8)$$

where N is a number of linear FE basis functions ϕ , $|e_l|$ is the electrode length and δ_{kl} is Kronecker delta.

For detailed information and derivation of individual terms, the interested reader is referred to [81, 21, 82] and literature therein.

4.2 General Transport Model (GTM) application

Following the same principles, one can generalize the concept for arbitrary transport process governed by diffusion equation. For the purpose of civil engineering application, we shall consider a steady state heat equation with its boundary conditions in a following form

$$\begin{cases} \nabla \cdot (\lambda(x) \nabla u(x)) = 0, & x \in \Omega \\ \lambda \frac{\partial u}{\partial n}(x) = \alpha^{(i)} (u_0^{(i)}(x) - u(x)), & x \in \partial\Omega_T^{(i)} \setminus e_l \\ u(x) + r_l \lambda \frac{\partial u}{\partial n}(x) = T_l, & x \in e_l \\ \lambda(x) \frac{\partial u}{\partial n}(x) = \tilde{f}_N, & x \in \partial\Omega_N^{(i)} \setminus e_l \end{cases} \quad (4.9)$$

$\partial\Omega^{(i)} = \partial\Omega_T^{(i)} \cup \partial\Omega_N^{(i)} \cup e_l, l = 1, \dots, L, \quad i = 1, \dots, I.$

In contrast to EIT, the potential $u(x)$ [K] represents a different physical quantity, i.e. a temperature field, therefore the electrodes e_l [–] now transforms into a thermocouples capable of varying its temperature instead of the electric current⁵. The other variables includes $\lambda(x)$ [$\text{W} \cdot \text{m}^{-1} \cdot \text{K}^{-1}$] which is a thermal conductivity field, L [–] is the total number of thermocouples, $r_l \in \mathbb{R}^L$ [$\text{K} \cdot \text{W}^{-1}$] is a thermocouple resistance coefficient and $T_l \in \mathbb{R}^L$ [K] is the l -th stimulation pattern. The environment factors are α [$\text{W} \cdot \text{m}^{-2} \cdot \text{K}^{-1}$] being the heat transfer coefficient, $u_0(x)$ [K] is the environment temperature and \tilde{f}_N [$\text{W} \cdot \text{m}^{-2}$] are prescribed fluxes.

The inputs for this model are then the conductivity field $\lambda(x)$, stimulation patterns $(T_l)_{l=1}^L \in \mathbb{R}^L$, contact resistances $(r_l)_{l=1}^L$ and the environmental

⁵Using Robin condition together with the thermocouple temperature T_l and transfer coefficient r_l , one can still use NTD map for GTM model.

factors $\alpha^{(i)}$, $u_0^{(i)}(x)$ and \tilde{f}_N . The model output consists of a temperature field $u(x)$ containing the whole boundary $\partial\Omega$.

Assumption 2. *The conductivity λ , contact resistances r_l and transfer coefficients $\alpha^{(i)}$ satisfy following*

- (i) $\lambda \in L^\infty(\Omega; \mathbb{R})$, $\inf_{x \in \Omega} \lambda(x) = \lambda_- > 0$,
- (ii) $0 < r_l^- \leq r_l \leq r_l^+ < \infty$, $l = 1, \dots, L$,
- (iii) $0 < \alpha_-^{(i)} \leq \alpha^{(i)} \leq \alpha_+^{(i)} < \infty$, $\forall i$.

Note one can omit conditions (iii) and (iv) in assumption 2 due to application of second and fourth condition in Eq. (4.9). This is due to the chosen boundary conditions, which already satisfy a more general consistency condition $\int_{\partial\Omega} \lambda \frac{\partial u}{\partial n} = 0$, meaning that the GTM model is more stable in comparison to CEM regardless the stimulation patterns.

Unlike in EIT, one do not have to rely only on measurements taken by thermocouples, but can actually choose an arbitrary part of boundary $\partial\Omega$, which can be understood as taking a thermal camera images. Also taking into account the reduced conditions according to assumptions 2, the *current stimulation pattern* translates into *temperature stimulation pattern* while still maintaining the NTD sensing given by Eq. (3.2). The temperature stimulation pattern can therefore take nearly arbitrary form, i.e. in the simplest case it could be expressed in a following way

$$T = T_e I = T_e \times \begin{bmatrix} 1 & 0 & \cdots & 0 \\ 0 & 1 & \cdots & 0 \\ \vdots & \vdots & \ddots & 0 \\ 0 & 0 & 0 & 1 \end{bmatrix}, \quad (4.10)$$

where T_e [K] is a constant temperature of an active thermocouple. Note that since the model stabilizes itself due to second condition in Eq. (4.9), one can stimulate just a single thermocouple in a time without dealing with the singularity of solution in the system of Eq. (4.9).

Numerical solution of the forward model

In contrast to CEM, the thermocouple potentials in GTM are given a priori, i.e. the thermocouples are driven by potential instead of flux, and therefore are not used for measurements which simplifies the forward operator solution.

$$F(\lambda) = \mathbf{u}_m, \quad \mathbf{u}_m \in \mathbb{R}^{M \cdot L}, \quad (4.11)$$

where \mathbf{u}_m are potential observed on boundary $\Gamma_m \subseteq \partial\Omega$ that is subjected to measurement, M is a cardinality of discrete form of Γ_m , i.e. number of FE nodes located on Γ_m and L is a number of thermocouples.

The individual vectors $\mathbf{u}^{(i)} \in \mathbb{R}^N$, $i = 1, \dots, L$ containing all potentials in Ω are obtained in a following way

$$(\mathbf{K}_u + \mathbf{K}_t^{(i)} + \mathbf{K}_e^{(i)}) \mathbf{u}^{(i)} = \tilde{\mathbf{f}}_t^{(i)} + \tilde{\mathbf{f}}_e^{(i)} + \tilde{\mathbf{f}}_n^{(i)}, \quad (4.12)$$

where the particular system matrices and corresponding right-hand side vectors are computed in a following way

$$K_{kl} = \int_{\Omega} \lambda \nabla \phi_k \cdot \nabla \phi_l \, dA \quad k, l = 1 \dots N \quad (4.13)$$

$$K_{t,kl}^{(i)} = \int_{\partial\Omega_T^{(i)}} \alpha^{(i)} \phi_k \phi_l \, dS \quad k, l = 1 \dots N \quad (4.14)$$

$$K_{e,kl}^{(i)} = \int_{e_l^{(i)}} \frac{1}{r_l^{(i)}} \phi_k \phi_l \, dS \quad k, l = 1 \dots N \quad (4.15)$$

$$\tilde{f}_{t,l}^{(i)} = \int_{\partial\Omega_T^{(i)}} \alpha^{(i)} u_0^{(i)} \phi_l \, dS \quad i = 1 \dots L, l = 1 \dots N \quad (4.16)$$

$$\tilde{f}_{e,l}^{(i)} = \int_{e_l^{(i)}} \frac{1}{r_l} T_l^{(i)} \, dS = \frac{|e_l|}{r_l} T_l^{(i)} \quad i = 1 \dots L, l = 1 \dots N \quad (4.17)$$

$$\tilde{f}_{n,l}^{(i)} = - \int_{\partial\Omega_N^{(i)}} \tilde{f}_N^{(i)} \phi_l \, dS \quad l = 1 \dots N \quad (4.18)$$

For detailed information and derivation of individual terms, the interested reader is referred to [6, 37, 74, 85] and literature therein.

4.3 Time dependent heat equation

In real conditions it is, however, not an easy task to sustain a stable and steady state conditions. Not only the surrounding temperature will fluctuate even in a laboratory environment, but for standard building materials like bricks, concrete, wood, etc. the steady state, after changing the loading conditions, can be reached after several hours or days depending on the volumetric capacity, heat conductivity and material thickness. Therefore, we intend to apply the identical principles used in a Calderón problem for time dependent models.

To capture a time dependent heat transfer, one can adopt following set of equations

$$\left\{ \begin{array}{l} \rho(x)c_p(x)\frac{\partial u}{\partial t}(x,t) - \nabla_{\mathbf{x}} \cdot (\lambda(x)\nabla_{\mathbf{x}}u(x,t)) = \tilde{f}(x,t), \quad x \in \Omega, t > 0 \\ \mathbf{n}(x) \cdot (\lambda(x)\nabla_{\mathbf{x}}u(x,t)) = \tilde{f}_N(x,t), \quad x \in \partial\Omega_N^{(i)} \\ \alpha^{(i)}(u(x,t) - u_0(x,t)) = \tilde{f}_T(x,t), \quad x \in \partial\Omega_T^{(i)} \\ u(x,t) = \tilde{f}_D(x,t), \quad x \in \partial\Omega_D^{(i)} \\ \partial\Omega^{(i)} = \partial\Omega_N^{(i)} \cup \partial\Omega_T^{(i)} \cup \partial\Omega_D^{(i)}, i = 1, \dots, I, \end{array} \right. \quad (4.19)$$

where ρ [$\text{kg} \cdot \text{m}^{-3}$] is volumetric mass density, c_p [$\text{J} \cdot \text{kg}^{-1} \cdot \text{K}^{-1}$] is specific heat capacity and $\partial\Omega_{(N,T,D)}^{(i)}$ are non-intersecting subsets of boundary $\partial\Omega^{(i)}$ in i -th loading condition with corresponding environmental factors u_0 [K], $\alpha^{(i)}$ [$\text{W} \cdot \text{m}^{-2} \cdot \text{K}^{-1}$], $\tilde{f}_{N,T}$ [$\text{W} \cdot \text{m}^{-2}$] and \tilde{f}_D [K].

In order to maintain NTD sensing, the set of equations in Eq. (4.19) is subjected to following constrain

Assumption 3. Let Γ_m be a subset of boundary $\partial\Omega$ that is subjected to measurements. Then

$$\Psi = \left(\partial\Omega_N^{(i)} \cup \partial\Omega_T^{(i)} \right) : (\Psi \cap \Gamma) \neq \emptyset, \forall i,$$

must hold, i.e. the boundary subjected to measurements must contain at least some Neumann conditions.

Another set of constrains similar to 2 and 1 is represented by following assumptions

Assumption 4. The material parameters λ , ρ , c_p and transfer coefficients $\alpha^{(i)}$ satisfy following

- (i) $\lambda \in L^\infty(\Omega; \mathbb{R})$, $\inf_{x \in \Omega} \lambda(x) = \lambda_- > 0$,
- (ii) $0 < \rho^- \leq \rho \leq \rho^+ < \infty$,
- (iii) $0 < c_p^- \leq c_p \leq c_p^+ < \infty$,
- (iv) $0 < \alpha_-^{(i)} \leq \alpha^{(i)} \leq \alpha_+^{(i)} < \infty$, $\forall i$.

In a definition of this model Eq. (4.19), one can notice that there is no mention of electrodes, thermocouples or measurements indicating our intention not to consciously intervene in the system itself, but only to rely on

external influences and a natural fluctuation of temperature throughout the day and night. For systems where their boundaries $\partial\Omega$ are not exposed to different external influences, one can adapt a similar techniques to GTM and CEM or control the ambient temperature in the second or third condition in equation Eq. (4.19).

A special feature of this model lies in its independence on excitation device, i.e. stimulation electrodes or thermocouples, and therefore has the least requirements on equipment and the full measurement setup consist of arrays of thermometers or two or more thermal cameras.

Numerical solution of the forward model

The forward operator F consists of two independent parameters and solves the system for all time steps N_t at once, giving rise to a following formulation

$$F(\lambda, c_v) = \mathbf{u}_m, \quad \mathbf{u}_m \in \mathbb{R}^{M \cdot N_t}, \quad (4.20)$$

where the inputs are heat conductivity λ and volumetric capacity $c_v = \rho \cdot c_p$. The measurement matrix $\mathbf{u}_m \in \mathbb{R}^{M \cdot N_t}$, where M is number of measurements within single time step and N_t is number of time steps, is obtained as a subset of complete solution vectors \mathbf{u}_i , $i = 1, \dots, N_t$ from a following set of linear equations

$$\begin{aligned} (\mathbf{C} + \tau \Delta t (\mathbf{K} + \mathbf{K}_t)) \mathbf{u}_{i+1} &= (\mathbf{C} - (1 - \tau) \Delta t (\mathbf{K} + \mathbf{K}_t)) \mathbf{u}_{i-1} + \dots \\ &\quad \Delta t \left((1 - \tau) \tilde{\mathbf{f}}_{n,i-1} + \tau \tilde{\mathbf{f}}_{n,i} \right) + \dots \\ &\quad \Delta t \left((1 - \tau) \tilde{\mathbf{f}}_{t,i-1} + \tau \tilde{\mathbf{f}}_{t,i} \right) + \dots \\ &\quad \Delta t \left((1 - \tau) \tilde{\mathbf{f}}_{d,i-1} + \tau \tilde{\mathbf{f}}_{d,i} \right), \end{aligned} \quad (4.21)$$

where $\Delta t = t_{i+1} - t_i$ is a time step, $\tau \in \langle 0; 1 \rangle$ is a time integration parameter⁶ and the system matrices and right hand side vectors are computed in a following way

$$K_{kl} = \int_{\Omega} \lambda \nabla \phi_k \cdot \nabla \phi_l \, dA \quad k, l = 1 \dots N \quad (4.22)$$

$$C_{kl} = \int_{\Omega} \rho c_p \phi_k \phi_l \, dA \quad k, l = 1 \dots N \quad (4.23)$$

$$K_{t,kl} = \int_{\partial\Omega_T} \alpha \phi_k \phi_l \, dS \quad k, l = 1 \dots N \quad (4.24)$$

⁶The foregoing computations were calculated using Crank-Nicolson integration method, i.e. $\tau = 0.5$

$$\tilde{f}_{t,li} = \int_{\partial\Omega_T} \alpha u_{0,i} \phi_l \, dS \quad i = 1 \dots N_t, l = 1 \dots N \quad (4.25)$$

$$\tilde{f}_{n,li} = - \int_{\partial\Omega_N} \tilde{f}_N(t_i) \phi_l \, dS \quad i = 1 \dots N_t, l = 1 \dots N \quad (4.26)$$

$$\tilde{\mathbf{f}}_{d,i} = -(\mathbf{K} + \mathbf{K}_t) \tilde{\mathbf{f}}_D(t_i) \quad i = 1 \dots N_t \quad (4.27)$$

For detailed information and derivation of individual terms, the interested reader is referred to [6, 37, 74, 85] and literature therein.

4.4 Numerical solution to the inverse problem

All results in section 5 share the same regularised Gauss-Newton (GN) iteration scheme in a following form

$$\sigma_{k+1} = \sigma_k + \delta\sigma_k, \quad (4.28)$$

$$\delta\sigma_k = \left(\mathbf{J}_k^T \mathbf{J}_k + \alpha_k \mathbf{L}^T \mathbf{L} \right)^{-1} \left(\mathbf{J}_k^T (\mathbf{u}_r - F(\sigma_k)) - \alpha_k \mathbf{L}^T \mathbf{L} (\sigma_k - \sigma_r) \right), \quad (4.29)$$

where $F(\sigma) \in \mathbb{R}^{vw}$ represents a discrete NTD operator of a forward model with v being the number of measurement points, i.e. a number of nodes of FE mesh on a subset Γ_v of boundary $\partial\Omega$ that is being measured and w is the number of experiments. The a priori measured quantity is stored in vector $\mathbf{u}_r \in \mathbb{R}^{vw}$ and the regularisation operator \mathbf{L} is a pre-calculated Laplacian of a piece-wise constant functions on a finite element mesh. In all cases the reference field $\sigma_r(\mathbf{x}) = \sigma_0(\mathbf{x}) = 1$ for $\mathbf{x} \in \Omega$.

From our experience, the most stable choice of hyper-parameter α_k was the one used in Levenberg-Marquardt regularisation (LMR) [58], which is gradually decreasing during the iteration and takes following form

$$\alpha_k = \max \left(\max \left(\mathbf{J}_k^T \mathbf{J}_k \right) \right). \quad (4.30)$$

Jacobian \mathbf{J}_k was updated in each iteration and was calculated numerically in a following way

$$J_i^{(jkl)} = \frac{\partial u_{jk}}{\partial \sigma_i^l}, \quad (4.31)$$

where \mathbf{J}_i is a third-order tensor in i -th iteration, indexes jk are representing measurement nodes in FE mesh and individual measurements respectively. Index l identifies a conductivity change on l -th FE element. The tensor is calculated numerically and matricised along indexes jk for calculation purposes.

Additional numerical treatment

As the iteration scheme Eq. (4.29) is fairly simple and does not include any supplementary constraints which are necessary for the solver robustness, one has to adopt further numerical treatment in order to maintain the assumptions 1 and 2 valid within the iteration. Introduction of the following two operators increased the stability and robustness of results substantially.

The constraint for strict positivity of conductivity field during the iteration is treated with an ad-hoc algorithm which is not allowing the occurrence of negative numbers and gives rise to a *positivity operator*, i.e. T_p in a following way

$$\tilde{\sigma}(x) = T_p(\sigma(x)) = \begin{cases} \sigma(x) > 0 \rightarrow x^+, & \text{then } \sigma(x^+) = \sigma(x^+), \\ \sigma(x) < 0 \rightarrow x^-, & \text{then } \sigma(x^-) = \min(\sigma(x^+)). \end{cases} \quad (4.32)$$

Since the problem is inherently non-linear and the iteration scheme proceeds with non-restricted linear steps we introduce a *cap operator* T_c limiting the resulting step size to a chosen value k in a following way

$$\delta\hat{\sigma}(x) = T_c(\delta\sigma(x)) = \begin{cases} \delta\sigma(x) > k, & \text{then } \delta\sigma(x) = \text{sign}(\delta\sigma(x)) \cdot k, \\ \delta\sigma(x) < k, & \text{then } \delta\sigma(x) = \delta\sigma(x). \end{cases} \quad (4.33)$$

The final modified GN iteration scheme after applying Eq. (4.32) and Eq. (4.33) operators to Eq. (4.28) then takes following form

$$\sigma_{k+1} = T_p(\sigma_k + T_c(\delta\sigma_k)). \quad (4.34)$$

5 Results

In this section we provide an insight into the performance of reconstruction algorithms under various conditions, i.e. limiting number of measurements, partial data reconstruction, different material properties and considering different domains.

First we show an implementation of a classical EIT procedure for medical imaging with electrodes capable of both sending and receiving signal, i.e. gathering data. The governing equation describes the underlying physics of electrostatics and therefore the ultimate goal is to recover an electrostatic conductivity field σ within domain Ω .

The second example comprises results gathered from GT-model simulating a steady state heat transfer, where only a few active thermocouples are placed on the accessible boundary of a domain of interest. In contrast to classical EIT settings, in GTM the thermocouples serve a single purpose, i.e. to excite different boundary conditions and are not meant to collect any kind of data although they could. The measurements are assumed to be conducted by thermal camera or by an array of discrete thermometers with appropriate interpolation providing continuous surface data. The main goal is to reconstruct the thermal conductivity λ inside the domain Ω .

From practical point of view, the most interesting model is represented by the time-dependent heat equation, which can capture even sudden changes in external factors and loading conditions during the observation. We assume changes in temperature on the observed boundary over several days can provide sufficient amount of data for the algorithm to recover material fields, i.e thermal conductivity λ and volumetric capacity c_v . In case the observed structure is located in an environment without sufficient changes in loading conditions, one may use a device that excites a different boundary conditions, e.g. a heater or air conditioning system.

The measure of reconstruction algorithm performance is represented by an error on the reconstructed material field in comparison to the original field in a following way

$$\varepsilon_\sigma = \frac{\|\sigma_{rec} - \sigma_{true}\|_2}{\|\sigma_{true}\|_2}, \quad (5.1)$$

where σ_{rec} is the recovered material field obtained as Eq. (4.34) and σ_{true} is the original material field.

If it is not mentioned otherwise, the reconstructed parameters for the first iteration of Eq. (4.34) are chosen as constant unit fields.

5.1 Electrical Impedance Tomography

In foregoing examples, we assume the classical settings of CEM model, where the electrode impedance, applied currents and domain dimensions with electrode placement Fig. 1, Fig. 4 are known. In the first case, we study the reconstruction algorithm performance for limited the number of measurement electrodes with a smooth Fig. 2 and a non-differentiable Fig. 3 material field.

All examples share the same electrode properties, i.e. the impedance z_l and applied current C takes following values

$$\begin{aligned} z_l &= 1, \forall l = 1, \dots, L, \\ C &= 1. \end{aligned} \quad (5.2)$$

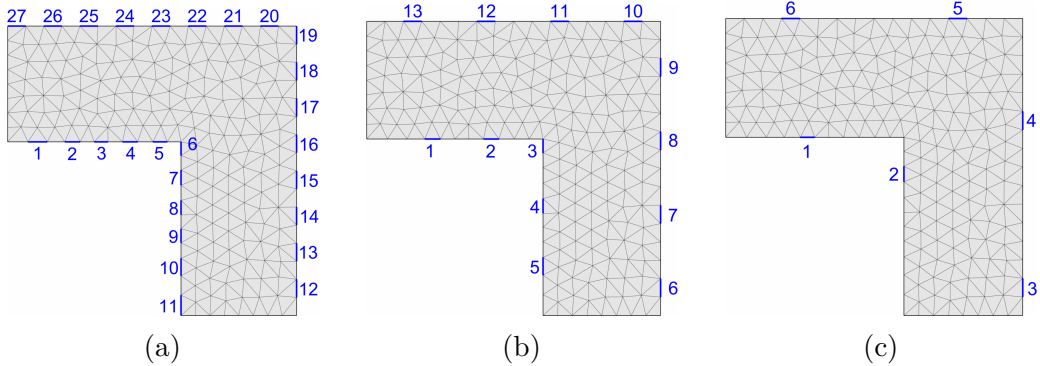


Figure 1: Domain set with limited number of measurement electrodes.

The corresponding results were computed using Eq. (4.34) and are shown in Fig. 2.

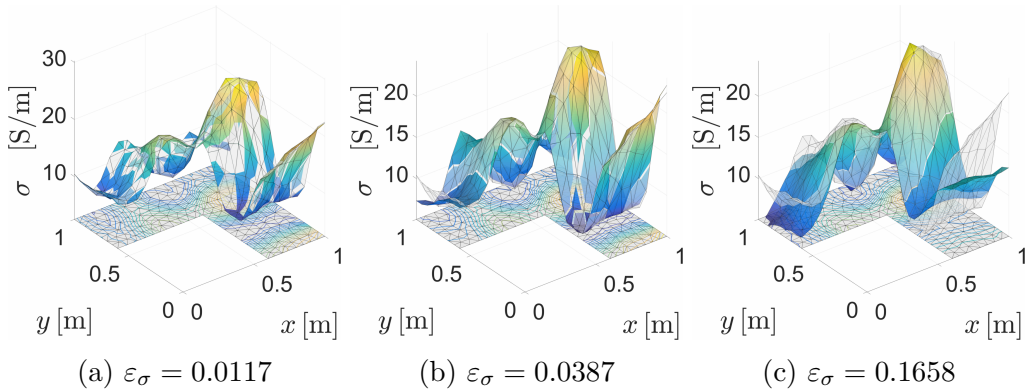


Figure 2: CEM reconstructed material fields with smooth material field. In colour: σ_{rec} , In grey: σ_{true}

In comparison to smooth material field Fig. 2, one can notice that non-differentiable reconstruction Fig. 3 suffer from insufficiency of data, i.e. in general the non-differentiability raise a need for more data in order to achieve the same precision.

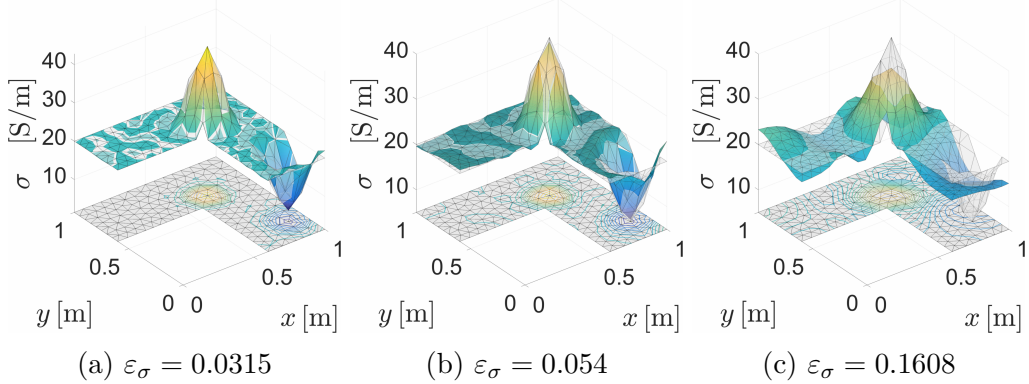


Figure 3: CEM reconstructed material fields with non-differentiable material field. In colour: σ_{rec} , In grey: σ_{true}

The second set of benchmark examples is dealing with material inclusions Fig. 4a, partial data reconstruction Fig. 4b and a combination of both Fig. 4c.

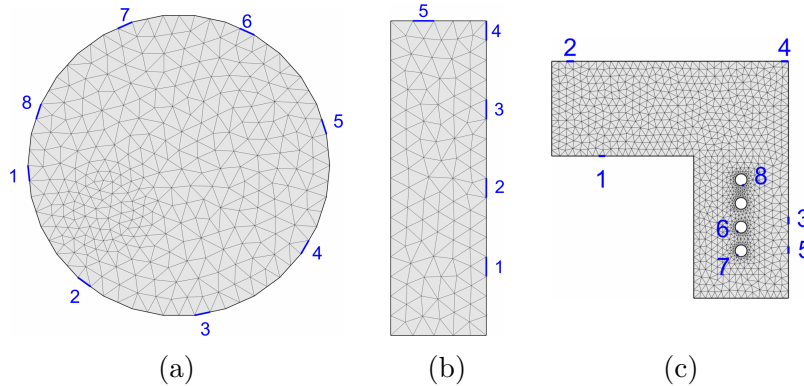


Figure 4: Domain set with limited number of measurement electrodes.

Corresponding results are shown in Fig. 5.

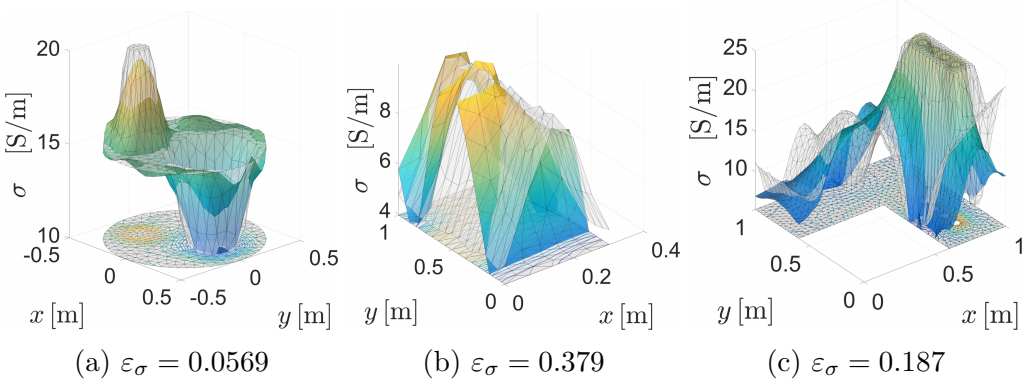


Figure 5: CEM reconstructed material fields with various material field. In colour: σ_{rec} , In grey: σ_{true}

In Fig. 5a, the shape is recovered nearly accurately except of sharp edges, which confirms the previous statement in section 2 that applying the 2-norm in minimisation functional favours smooth transitions. When the information is completely missing, i.e. Fig. 5b, the reconstruction perform poorly, the resulting field is of dubious quality and in general the algorithm behaves rather unpredictably. For complex geometry with missing information in Fig. 5c, one can notice the resulting field was exemplary smoothed out.

5.2 General Transport Model

In the first set of examples with domain, measurements and thermocouples placement shown in Fig. 6, we assume the steady state is induced by boundary conditions

$$\begin{aligned} \lambda \frac{\partial u}{\partial n}(x)|_{\partial\Omega_1} &= 10 \cdot (30 - u(x)), \\ \lambda \frac{\partial u}{\partial n}(x)|_{\partial\Omega_2} &= 10 \cdot (15 - u(x)). \end{aligned} \quad (5.3)$$

The following examples are configured in such a way to verify the performance and stability when the model is subjected to substantially constrained measurements with two different material fields. In Fig. 6 the observed boundaries are emphasised with red dots, whereas electrodes are displayed as blue lines⁷. The corresponding results for smooth and non-differentiable material fields are shown in Fig. 7 and Fig. 8 respectively.

⁷Notice there are only two thermocouples, resulting into two states, i.e. loading conditions, and hence two measurements are made.

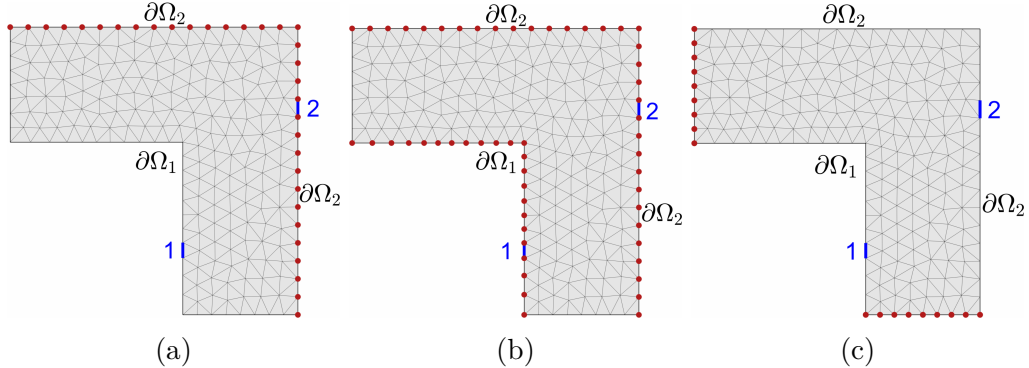


Figure 6: Domain set with two thermocouples (blue) and observed boundaries (red).

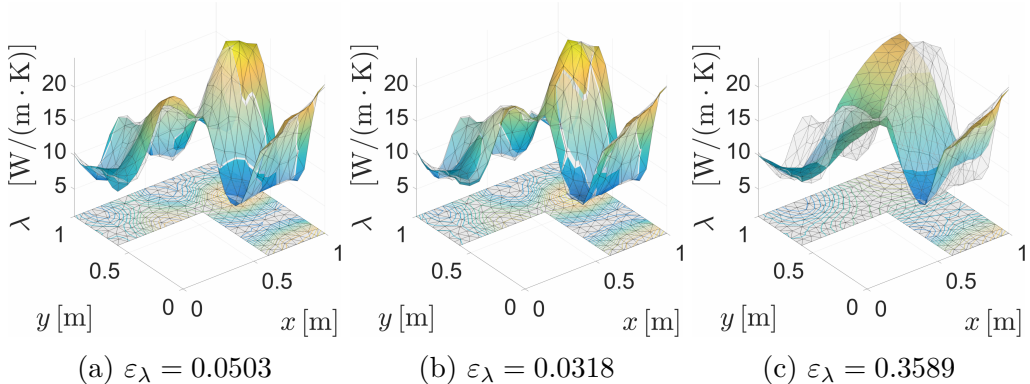


Figure 7: GTM reconstructed material fields with smooth material field. In colour: λ_{rec} , In grey: λ_{true}

The most interesting result is that there is visually almost no difference between Fig. 7b and Fig. 7a although the latter employs nearly half the measurement nodes and the information about the state variable on $\partial\Omega_1$ is completely missing. It is the result of combining domain shape, chosen measurements⁸ and material properties, i.e. smoothness.

⁸Imagine one can bend the domain to a doughnut shape maintaining the measurements on the outer boundary. Then the measurements provide a complete information about the material properties inside the domain

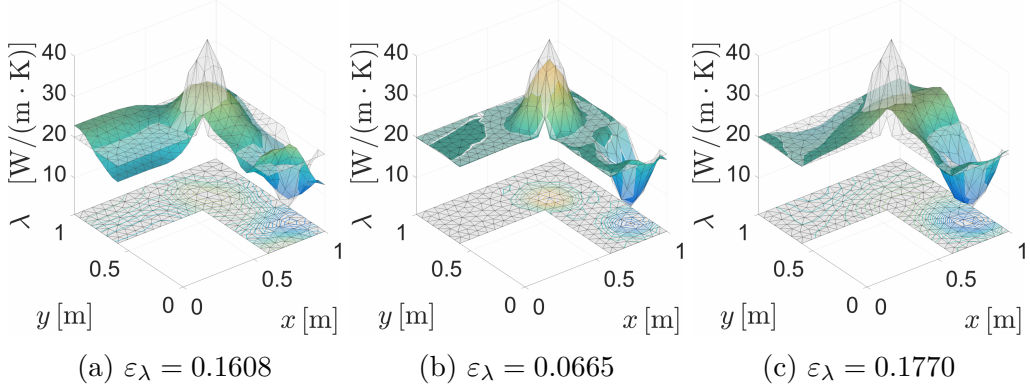


Figure 8: GTM reconstructed material fields with non-differentiable material field. In colour: λ_{rec} , In grey: λ_{true}

Similar to the previous example in CEM, one can observe a significant deterioration of results in Fig. 8 when the underlying material field is non-differentiable.

The second set of examples comprises a partial data reconstruction on a circular shape domain with two inclusions Fig. 9a, a direction biased partial data reconstruction Fig. 9b and a more complex geometry and material recovery Fig. 9c. The steady state is induced by boundary conditions

$$\begin{aligned} \lambda \frac{\partial u}{\partial n}(x)|_{\partial\Omega_1} &= 10 \cdot (30 - u(x)) \\ \lambda \frac{\partial u}{\partial n}(x)|_{\partial\Omega_2} &= 10 \cdot (15 - u(x)) \end{aligned} \quad (5.4)$$

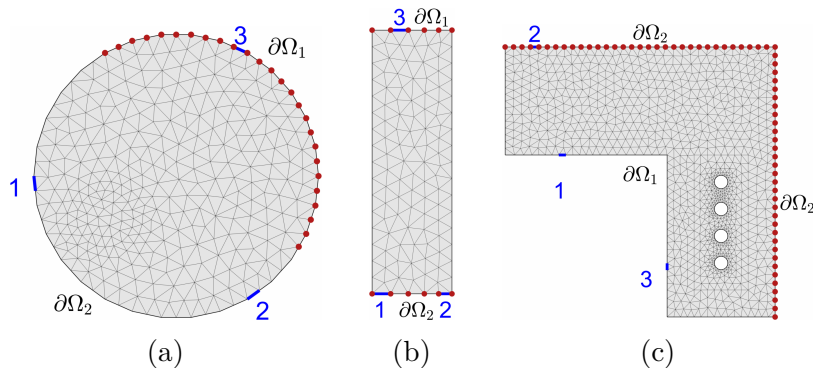


Figure 9: Domain set with three thermocouples (blue) and observed boundaries (red).

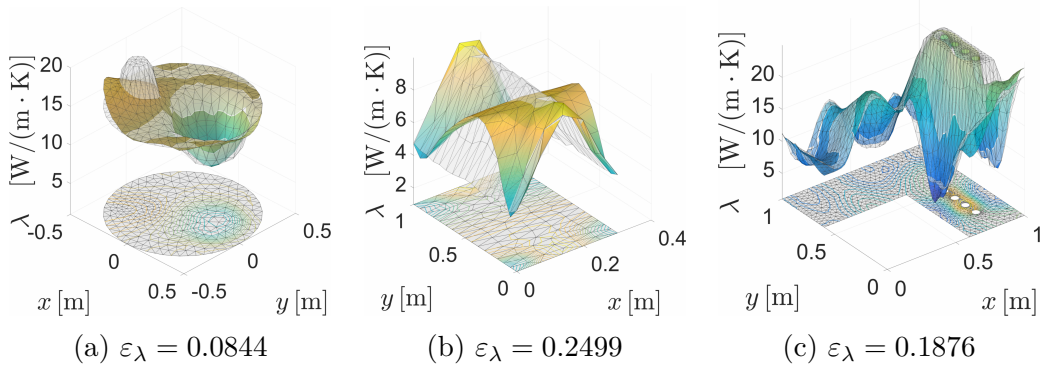


Figure 10: GTM reconstructed material fields with various material fields.
In colour: λ_{rec} , In grey: λ_{true}

In Fig. 10a one can notice the combination of particular domain shape with a choice of measurements can be of critical importance. Even though approximately 43% of boundary was observed, the second material inclusion could not be fully recovered. In the second example on Fig. 10b, the observed boundary together with thermocouples and load conditions were aligned in such a way that they could provide an information only in a single direction, thanks to which the medium can not be recovered properly. The last L-shaped domain is a similar example to the Fig. 7a with a more complex geometry and material distribution. Despite the decreased accuracy the reconstruction with substantial part of boundary missing can still lead to satisfactory results.

5.3 Time dependent heat equation

Next example consider structural detail considering a corner of a building made of light concrete with inhomogeneities subjected to measurements. The structure was monitored for 10 days in its natural environment which translates into following boundary conditions

$$\lambda \frac{\partial u}{\partial n}(x, t)|_{\partial \Omega_i} = 10 \cdot (u(x, t) - f_i(t)), \quad (5.5)$$

where f_i is a function of time and is shown in Fig. 11b.

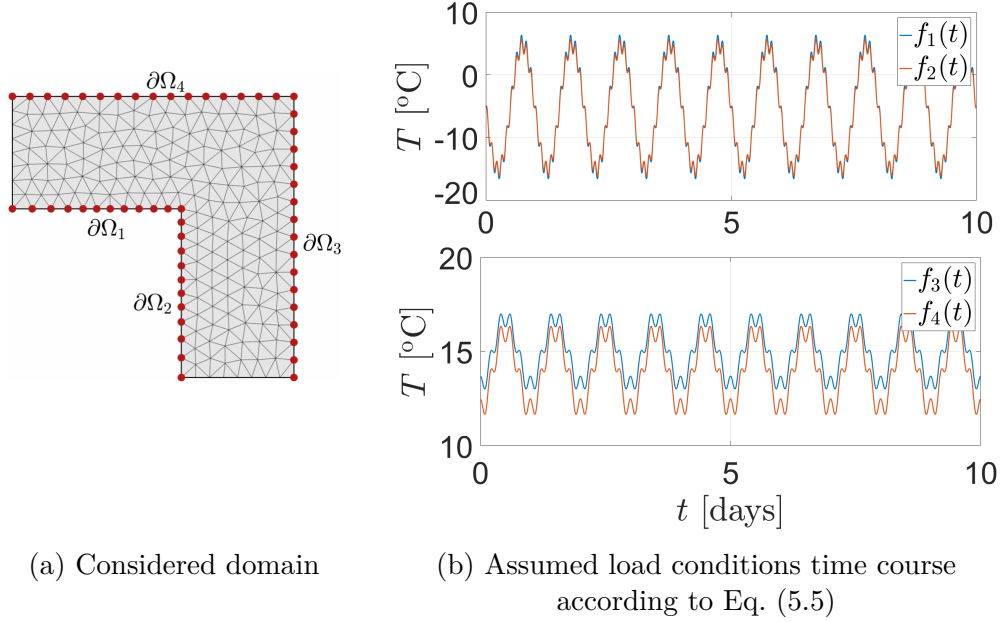


Figure 11

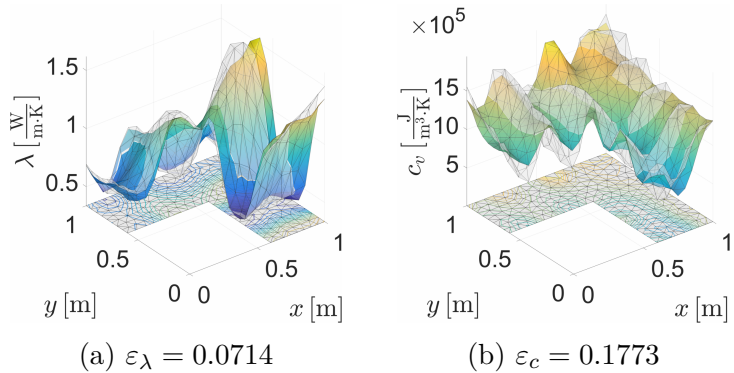


Figure 12: Time dependent model reconstructed material fields with smooth material field. In colour: λ_{rec} , $c_{v,rec}$, In grey: λ_{true} , $c_{v,true}$.

Even though the measurements contain a huge amount of redundant information, the results actually show the possibility of recovering parameters of parabolic equation. The quality of reconstruction can be further improved by providing the calculation with a more variable data, e.g. using air conditioning, heaters, etc.

6 Summary and future work

In this thesis, we recapitulated the standard procedure of EIT used in medical imaging, extended with analysis of partial data reconstruction, which is discussed in section 5. The problem was further reformulated for the purpose of general transport model (GTM) driven by linear elliptic equation, i.e. heat transport, groundwater flow, electrostatics, etc. in section 4. The GTM results for partial data reconstruction, various domain shapes and material properties were numerically verified in section 5. Finally, we introduced and studied a time dependent transport model with an example considering a realistic material properties in a detail representing a corner of a building. Solutions to the inverse problem were obtained using a deterministic approach, namely regularised Gauss-Newton method with LMR strategy for decreasing the regularisation parameter.

Despite the inaccuracies in certain situations, e.g. insufficiency of data, non-smooth material field, the Gauss-Newton method proved to be stable and flexible solver for such tasks. It showed it can handle reconstruction with a very limited data for CEM and GTM for various domains and material properties.

Also from the results, it is apparently possible to recover parameters of a linear parabolic differential equation, which opens up possibilities in a wide range of application in Civil Engineering and other fields.

The future work include an implementation of a different solver based on a Bayesian inference with the possibility to naturally consider the measurement errors and provide even further stability and control over the reconstructed parameter. An important step is to use a different mesh for simulating the observed measurements and for the reconstruction process in order not to get biased by using the similar mesh which should be also avoided [35]. A bit more challenging task will be to employ a more complicated non-linear time dependent model describing coupled heat and moisture transport instead of a simple two-parameter linear heat transfer.

References

- [1] G. Alessandrini and M. Di Cristo. Stable determination of an inclusion by boundary measurements. *SIAM journal on mathematical analysis*, 37(1):200–217, 2005.
- [2] A. Allers and F.I Santosa. Stability and resolution analysis of a linearized problem in electrical impedance tomography. *Inverse problems*, 7(4):515, 1991.
- [3] K. Y. Aristovich, B. C. Packham, H. Koo, G. S. Santos, A. McEvoy, and D. S. Holder. Imaging fast electrical activity in the brain with electrical impedance tomography. *NeuroImage*, 124, Part A:204 – 213, 2016.
- [4] K. Astala, L. Päivärinta, and M. Lassas. Calderóns' inverse problem for anisotropic conductivity in the plane. *Communications in Partial Differential Equations*, 30(1-2):207–224, 2005.
- [5] D. C. Barber and B. H. Brown. Applied potential tomography. *Journal of Physics E: Scientific Instruments*, 17(9):723, 1984.
- [6] K. J. Bathe. *Finite element procedures*. Klaus-Jurgen Bathe, 2006.
- [7] Z. P. Bažant, Z. Bittnar, M. Jirásek, and J. Mazars. *Fracture and Damage in Quasibrittle Structures: Experiment, modeling and computation*. CRC Press, 2004.
- [8] Z. P. Bažant and R. L'Hermite. *Mathematical modeling of creep and shrinkage of concrete*. Wiley New York, 1988.
- [9] C. A. Berenstein and T. E. Casadio. Inversion formulas for the k -dimensional radon transform in real hyperbolic spaces. *Duke Mathematical Journal*, 62(3):613–631, 04 1991.
- [10] J. Bikowski, K. Knudsen, and J. L. Mueller. Direct numerical reconstruction of conductivities in three dimensions using scattering transforms. *Inverse Problems*, 27(1):015002, 2010.
- [11] R. Blue. *Real-time three-dimensional electrical impedance tomography*. Phd thesis, R.P.I, Troy, 1997.
- [12] R. S. Blue, D. Isaacson, and J. C. Newell. Real-time three-dimensional electrical impedance imaging. *Physiological measurement*, 21(1):15, 2000.

- [13] A. Borsic, W. R. B. Lionheart, and C. N. McLeod. Generation of anisotropic-smoothness regularization filters for EIT. *IEEE Transactions on Medical Imaging*, 21(6):579–587, June 2002.
- [14] Andrea Borsic, Brad M Graham, Andy Adler, and William RB Lionheart. In vivo impedance imaging with total variation regularization. *IEEE transactions on medical imaging*, 29(1):44–54, 2010.
- [15] B. H. Brown, D. C. Barber, and A. D. Seagar. Applied potential tomography: Possible clinical applications. *Clinical Physics and Physiological Measurement*, 6(2):109, 1985.
- [16] R. M. Brown and G. A. Uhlmann. Uniqueness in the inverse conductivity problem for nonsmooth conductivities in two dimensions. *Communications in Partial Differential Equations*, 22(5-6):1009–1027, 1997.
- [17] A. P. Calderón. On an inverse boundary value problem. *Seminar on Numerical Analysis and Its Applications to Continuum Physics: Rio de Janeiro*, 12:67–73, 1980.
- [18] A. P. Calderón. On an inverse boundary value problem. *Computational & Applied Mathematics*, 25:133 – 138, 00 2006.
- [19] S. Campana and S. Piro. *Seeing the Unseen Geophysics and Landscape Archaeology*. Taylor & Francis, 2008.
- [20] M. Cheney, D. Isaacson, J. C. Newell, S. Simske, and J. Goble. NOSER: An algorithm for solving the inverse conductivity problem. *International Journal of Imaging Systems and Technology*, 2(2):66–75, 1990.
- [21] K. S. Cheng, D. Isaacson, J. C. Newell, and D. G. Gisser. Electrode models for electric current computed tomography. *IEEE Transactions on Biomedical Engineering*, 36(9):918–924, 1989.
- [22] V. Cherepenin, A. Karpov, A. Korjenevsky, V. Kornienko, A. Mazaletskaya, D. Mazourov, and D. Meister. A 3D electrical impedance tomography (EIT) system for breast cancer detection. *Physiological Measurement*, 22(1):9, 2001.
- [23] M. H. Choi, T. J. Kao, D. Isaacson, G. J. Saulnier, and J. C. Newell. A simplified model of mammography geometry for breast cancer imaging with electrical impedance tomography. In *The 26th Annual International Conference of the IEEE Engineering in Medicine and Biology Society*, volume 1, pages 1310–1313, Sept 2004.

- [24] D. Colton and R. Kress. *Inverse acoustic and electromagnetic scattering theory*, volume 93. Springer Science & Business Media, 2012.
- [25] T. Dai and A. Adler. Electrical impedance tomography reconstruction using L1 norms for data and image terms. In *Engineering in Medicine and Biology Society, 2008. EMBS 2008. 30th Annual International Conference of the IEEE*, pages 2721–2724. IEEE, 2008.
- [26] W. Daily, A. Ramirez, D. LaBrecque, and W. Barber. Electrical resistance tomography experiments at the oregon graduate institute. *Journal of Applied Geophysics*, 33(4):227 – 237, 1995.
- [27] W. Daily, A. Ramirez, D. LaBrecque, and J. Nitao. Electrical resistivity tomography of vadose water movement. *Water Resources Research*, 28(5):1429–1442, 1992.
- [28] J. B. Drake. *Climate Modeling for Scientists and Engineers*. SIAM, 2014.
- [29] R. G. Ghanem and P. D. Spanos. Stochastic finite elements: a spectral approach, 2003.
- [30] B. M. Graham. *Enhancements in Electrical Impedance Tomography (EIT) Image Reconstruction for 3D Lung Imaging*. Phd thesis, School of Information Technology, University of Ottawa, 2007.
- [31] A. Greenleaf, M. Lassas, and G. Uhlmann. Anisotropic conductivities that cannot be detected by EIT. *Physiological Measurement*, 24(2):413, 2003.
- [32] Ch. W. Groetsch. *Inverse problems in the mathematical sciences*, volume 52. Springer, 1993.
- [33] S. J. Hamilton, M. Lassas, and S. Siltanen. A direct reconstruction method for anisotropic electrical impedance tomography. *Inverse Problems*, 30(7):075007, 2014.
- [34] R. P. Henderson and J. G. Webster. An impedance camera for spatially specific measurements of the thorax. *IEEE Transactions on Biomedical Engineering*, BME-25(3):250–254, May 1978.
- [35] D. S. Holder. *Electrical Impedance Tomography: Methods, History and Applications (Series in Medical Physics and Biomedical Engineering)*. Series in Medical Physics and Biomedical Engineering. Taylor & Francis, 1st edition, 2004.

- [36] S. M. Huang, A. B. Plaskowski, C. G. Xie, and M. S. Beck. Capacitance-based tomographic flow imaging system. *Electronics Letters*, 24(7):418–419, March 1988.
- [37] T. J. R. Hughes. *The finite element method: linear static and dynamic finite element analysis*. Courier Corporation, 2012.
- [38] A. J. Jaworski and T. Dyakowski. Application of electrical capacitance tomography for measurement of gas-solids flow characteristics in a pneumatic conveying system. *Measurement Science and Technology*, 12(8):1109, 2001.
- [39] M. Jirásek and Z. P. Bažant. *Inelastic analysis of structures*. John Wiley & Sons, 2002.
- [40] C. Kenig and M. Salo. The Calderón problem with partial data on manifolds and applications. *Analysis & PDE*, 6(8):2003–2048, 2014.
- [41] C. E. Kenig, J. Sjöstrand, and G. Uhlmann. The Calderón problem with partial data. *Annals of Mathematics*, 165(2):567–591, 2007.
- [42] A. Kirsch. *An Introduction to the Mathematical Theory of Inverse Problems*. Applied Mathematical Sciences 120. Springer-Verlag New York, 2 edition, 2011.
- [43] K. Knudsen. The Calderón problem with partial data for less smooth conductivities. *Communications in Partial Differential Equations*, 31(1):57–71, 2006.
- [44] K. Knudsen, M. Lassas, J. L. Mueller, and S. Siltanen. Regularized D-bar method for the inverse conductivity problem. *Inverse Problems and Imaging*, 3(4):599–624, 2009.
- [45] H. M. Künzel. *Simultaneous Heat and Moisture Transport in Building Components*. PhD thesis, Fraunhofer Institute of Building Physics, 1995.
- [46] V. Kolehmainen. *Novel approaches to image reconstruction in diffusion tomography*. Phd thesis, Kuopion University, 2001.
- [47] C. Lanczos. *Linear Differential Operators*. Society for Industrial and Applied Mathematics, 1996.
- [48] R. E. Langer. An inverse problem in differential equations. *Bulletin of the American Mathematical Society*, 39(10):814–820, 10 1933.

- [49] S. Leonhardt and B. Lachmann. Electrical impedance tomography: the holy grail of ventilation and perfusion monitoring? *Intensive Care Medicine*, 38(12):1917–1929, 2012.
- [50] W. R. B. Lionheart. Conformal uniqueness results in anisotropic electrical impedance imaging. *Inverse Problems*, 13(1):125, 1997.
- [51] W. K. Liu, A. Mani, and T. Belytschko. Finite element methods in probabilistic mechanics. *Probabilistic Engineering Mechanics*, 2(4):201 – 213, 1987.
- [52] Y. Mamatjan, A. Borsic, D. Gürsoy, and A. Adler. Experimental/clinical evaluation of EIT image reconstruction with ℓ_1 data and image norms. *Journal of Physics: Conference Series*, 434(1):012078, 2013.
- [53] H. G. Matthies, A. Litvinenko, B. V. Rosic, and E. Zander. Bayesian parameter estimation via filtering and functional approximations. *arXiv preprint arXiv:1611.09293*, 2016.
- [54] J. L. Melsa and D. L. Cohn. *Decision and estimation theory*. New York : McGraw-Hill, 1978.
- [55] J. L. Mueller, D. Isaacson, and J. C. Newell. Reconstruction of conductivity changes due to ventilation and perfusion from EIT data collected on a rectangular electrode array. *Physiological Measurement*, 22(1):97, 2001.
- [56] J. L. Mueller and S. Siltanen. Direct reconstructions of conductivities from boundary measurements. *SIAM Journal on Scientific Computing*, 24(4):1232–1266, 2003.
- [57] A. I. Nachman. Global uniqueness for a two-dimensional inverse boundary value problem. *Annals of Mathematics*, 143(1):71–96, 1996.
- [58] H. Niu, P. Guo, L. Ji, Q. Zhao, and T. Jiang. Improving image quality of diffuse optical tomography with a projection-error-based adaptive regularization method. *Optics express*, 16(17):12423–12434, 2008.
- [59] M. Noel and B. Xu. Archaeological investigation by electrical resistivity tomography: a preliminary study. *Geophysical Journal International*, 107(1):95, 1991.
- [60] E. R. Pike, J. G. McWhirter, M. Bertero, and Ch. de Mol. Generalised information theory for inverse problems in signal processing. In *IEE*

Proceedings F (Communications, Radar and Signal Processing), volume 131, pages 660–667. IET, 1984.

- [61] K. Prasad and R. B. Howard. Coupled fire dynamics and thermal response of complex building structures. *Proceedings of the Combustion Institute*, 30(2):2255 – 2262, 2005.
- [62] Leonid I Rudin, Stanley Osher, and Emad Fatemi. Nonlinear total variation based noise removal algorithms. *Physica D: Nonlinear Phenomena*, 60(1-4):259–268, 1992.
- [63] M. Salo. Calderón problem, 2008.
- [64] F. Santosa. *Inverse problems of acoustic and elastic waves*, volume 14. SIAM, 1984.
- [65] F. Santosa and M. Vogelius. A backprojection algorithm for electrical impedance imaging. *SIAM Journal on Applied Mathematics*, 50(1):216–243, 1990.
- [66] O. Scherzer. *Handbook of Mathematical Methods in Imaging*. Springer-Verlag New York, 2 edition, 2015.
- [67] S. Siltanen, J. Mueller, and D. Isaacson. An implementation of the reconstruction algorithm of A. Nachman for the 2d inverse conductivity problem. *Inverse Problems*, 16(3):681, 2000.
- [68] L. D. Slater, A. Binley, and D. Brown. Electrical imaging of fractures using ground-water salinity change. *Ground Water*, 35(3):436–442, 1997.
- [69] L. B. Slichter. The interpretation of the resistivity prospecting method for horizontal structures. *Physics*, 4(9):307–322, 1933.
- [70] J. Snoek, H. Larochelle, and R. P. Adams. Practical bayesian optimization of machine learning algorithms. In *Advances in neural information processing systems*, pages 2951–2959, 2012.
- [71] E. Somersalo, M. Cheney, and D. Isaacson. Existence and uniqueness for electrode models for electric current computed tomography. *SIAM Journal on Applied Mathematics*, 52(4):1023–1040, 1992.
- [72] E. Somersalo, M. Cheney, D. Isaacson, and E. Isaacson. Layer stripping: a direct numerical method for impedance imaging. *Inverse problems*, 7(6):899, 1991.

- [73] E. Somersalo, J. P. Kaipio, M. J. Vauhkonen, D. Baroudi, and S. Järvenpää. Impedance imaging and Markov chain Monte Carlo methods. In *Optical Science, Engineering and Instrumentation'97*, pages 175–185. International Society for Optics and Photonics, 1997.
- [74] G. Strang and G. J. Fix. *An analysis of the finite element method*, volume 212. Prentice-hall Englewood Cliffs, NJ, 1973.
- [75] J. Sylvester and G. Uhlmann. A uniqueness theorem for an inverse boundary value problem in electrical prospection. *Communications on Pure and Applied Mathematics*, 39(1):91–112, 1986.
- [76] J. Sylvester and G. Uhlmann. A global uniqueness theorem for an inverse boundary value problem. *Annals of Mathematics*, 125(1):153–169, 1987.
- [77] N. M. Tanushev and L. A. Vese. A piecewise-constant binary model for electrical impedance tomography. *Inverse Problems and Imaging*, 1(2):423, 2007.
- [78] A. Tarantola. *Inverse problem theory and methods for model parameter estimation*. SIAM, 2005.
- [79] T. Tidswell, A. Gibson, R. H. Bayford, and D. S. Holder. Three-dimensional electrical impedance tomography of human brain activity. *NeuroImage*, 13(2):283 – 294, 2001.
- [80] M. Th. Van Genuchten. A closed-form equation for predicting the hydraulic conductivity of unsaturated soils. *Soil science society of America journal*, 44(5):892–898, 1980.
- [81] M. Vauhkonen. *Electrical impedance tomography and prior information*. Phd thesis, Kuopio University, 1997.
- [82] M. Vauhkonen, W. R. B. Lionheart, L. M. Heikkinen, P. J. Vauhkonen, and J. P. Kaipio. A MATLAB package for the EIDORS project to reconstruct two-dimensional eit images. *Physiological Measurement*, 22(1):107, 2001.
- [83] A. J. Wilkinson, E. W. Randall, D. Durrett, T. Naidoo, and J. J. Cilliers. The design of a 1000 frames/second ERT data capture system and calibration techniques employed. In *3rd World Congress on Industrial Process Tomography*. Banff, 2003.

- [84] W. Q. Yang and L. Peng. Image reconstruction algorithms for electrical capacitance tomography. *Measurement Science and Technology*, 14(1):R1, 2003.
- [85] O. C. Zienkiewicz and R. L. Taylor. *The finite element method*, volume 3. McGraw-hill London, 1977.